Frontiers of Physics
https://doi.org/10.1007/s11467-020-0953-9
Front. Phys.
15(3), 33601 (2020)

RESEARCH ARTICLE

Mechanically scanned leaky-wave antenna based on a topological one-way waveguide

Qian Shen[1,2,3], Yun You[2], Jie Xu[2], Yun Shen[2], Xiaohua Deng[2], Zhuoyuan Wang[4], Weidong Min[5,†], Linfang Shen[6], Sanshui Xiao[3,‡]

[1] *Information Engineering School, Nanchang University, Nanchang 330031, China*
[2] *Institute of Space Science and Technology, Nanchang University, Nanchang 330031, China*
[3] *Department of Photonics Engineering, Technical University of Denmark, DK-2800 Kgs. Lyngby, Denmark*
[4] *Electronic and Information Engineering College, Ningbo University of Technology, Ningbo 315016, China*
[5] *School of Software, Nanchang University, Nanchang 330031, China*
[6] *Department of Applied Physics, Zhejiang University of Technology, Hangzhou 310023, China*
Corresponding authors. E-mail: [†]minweidong@ncu.edu.cn, [‡]saxi@fotonik.dtu.dk
Received November 28, 2019; accepted January 5, 2020

We propose a uniform backfire-to-endfire leaky-wave antenna (LWA) based on a topological one-way waveguide under external bias magnetic field. We systematically analyze the dispersion, showing that the proposed structure supports leaky mode arisen from total internal reflection. By means of tuning frequency or magnetic field, we obtain fixed-bias frequency and fixed-frequency bias LWA with continuous beam scanning from backward, broadside to forward direction. More importantly, we, for the first time, demonstrate that this proposed LWA shows mechanical tunability, allowing us to manipulate the radiation direction from backward, broadside to forward direction by mechanically tuning the air layer thickness. The simulated results show that our system exhibits super low 3dB beam width, high radiation efficiency as well as high antenna gain. Being provided such multiple controlled (especially mechanically) beam scanning manners, the present LWA paves an advanced approach for continuous beam scanning, holding a great potential for applications in modern communication and radar system.

Keywords leaky-wave antenna, one-way waveguide, magneto-optic materials

1 Introduction

Leaky-wave antenna (LWA) was firstly proposed as a slotted rectangular waveguide, in which the propagating waves can be leaked out in a specific angle when they are fast waves [1]. Because of the unique leaky property and beam scanning feature, LWAs can be widely used in various important applications, such as radar and satellite communications [2], conformal antennas [3] and microwave integrated systems [4, 5]. Some efforts based on quasi-uniform and periodic-structure antennas have been made towards achieving LWAs [6–8], where forward and backward beam scanning is induced yet no broadside beam scanning is found. Later, lots of brilliant works, including metamaterial assisted antenna [9], surface plasmon polaritons waveguide [10] and composite right/left-handed (CRLH) transmission line [10, 11], have cleared the hurdle to achieve broadside beam scanning, yet remaining a challenge of complicated constructions. Uniform antennas give us an opportunity to reduce the complexity, which still lack backward and broadside scanning [12, 13].

On the other hand, the beam scanning manners of LWAs in the previous works are characterized by changing the working frequency [6–13]. Recently, LWAs enabled fixed frequency scanning have received much attention, and different schemes have been proposed to realize continuous scanning by varying dc bias voltage at a fixed frequency [14–17]. In these research studies, fixed-frequency beam scanning is attained by loading varicap or capacitor, showing a maximum scanning angle of 80 degrees from backward, broadside to forward. However, it is challenging to set varactor diodes and add dc bias in practice. By introducing ferrite material such as yttrium iron garnet (YIG), which has tunable properties for microwave regime under an applied dc magnetic field [18, 19], some researchers found a positive chance to achieve fixed-frequency beam scanning with respect to broadside scanning [20]. It is reported that the ferrite material and left-handed concepts can be combined as microstripline [21, 22]; such structures exhibit broadside scanning yet are still involved in lacking fixed-frequency beam scanning and periodical unit cells. Compared to individual beam scanning assisted LWAs, LWAs with multiple scanning manners are preferable for applications in mordern communication. Recently, a uniform ferrite-loaded backfire-to-endfire LWA with CRLH response is first proposed relying on a magneto-optical waveguide [23, 24] under external

© Higher Education Press and Springer-Verlag GmbH Germany, part of Springer Nature 2020

magnetic field, where the backward propagation mode is suppressed. The use of the external magnetic field enables us to realize topological phase by breaking time-reversal symmetry, so-called quantum Hall effect [25–27], which is one of the three major classes of topological phases. Utilizing topolgical one-way waveguide provides a simple structure to obtain fixed-frequency bias and fixed-bias frequency beam scanning [28]. However, this structure utilizes an approximation of perfect magnetic conductor, which is difficult to build in practice.

In this paper, we propose a uniform LWA with backfire-to-endfire beam scanning, which relies on novel mechanically controlling at a fixed frequency. The leaky part of the proposed LWA is composed of a metal-air-YIG-air (MAYA) waveguide under bias magnetic field. We systemically analyze the dispersion of the leaky part, showing that leaky mode is guided by the zigzag reflections at the metal surface and upper YIG-air interface. Our structure supports not only fixed-bias frequency sweep but also fixed-frequency bias sweep from backward, broadside, to forward directions. More importantly, our structure can achieve backfire-to-endfire scanning by manipulating air thickness at fixed-frequency and fixed-bias, which is the first and unique structure exhibiting mechanically scanned feature to the best of our knowledge. It is shown that the beam scanning range reaches as high as 149°, low average 3 dB beam width of 4.6°, and the radiation efficiency value is up to 94% with maximum gain of 23 dBi. Different from the previous complex and well-designed periodical structure, the air thickness in our uniform and layered structure is straightforward to engineer by simply moving the upper metal layer. Besides regular fixed-bias and fixed-frequency beam scanning, our LWA with simple structure also provide an advanced beam scanning manner of mechanically controlling, exhibiting a great potential for various applications in modern communication and radar system.

2 Proposed structure and mode analysis

The schematic of the proposed mechanically scanned Leaky-wave antenna composed of three systems (I, II and III) is shown in Fig. 1(a), where the red dashed frame is the main leaky structure with the length of L. Systems I and III are one-way waveguide consisting of metal-air-YIG-metal discussed detailed in our recently published paper [29], which supports one-way propagating modes without back reflection, while system II, corresponding to the main leaky structure, is a four-layered meal-air-YIG-air (MAYA) waveguide introduced in this paper. A rectangular transverse-electric-polarized (TE) mode is coupled into the left-end of system I, then it travels and radiates to the lower air layer through the thin YIG layer in system II, finally the remaining wave propagates into system III. The upper metal layer is designed to be movable so that we can manipulate the air thickness straightforwardly and conveniently. Moreover, the present two-dimensional (2D) system can be extended to a realistic three-dimensional (3D) system with width w, see Fig. 1(b), which is uniform in the x direction and terminated by a pair of metal slabs. The electric fields of propagating mode in such uniform 3D system satisfy the boundary conditions in the lateral direction, consequently the fields in the 3D system are equivalent to those in the 2D system in physics. The metal in Fig. 1 is assumed to be perfect electric conductor (PEC), which is a reasonable approximation at microwave regime. The air layer with thickness d_a has the relative permittivity $\epsilon_a = 1$ and the YIG layer with thickness d_y has the relative permittivity $\epsilon_y = 15$. In our system, a bias dc magnetic field H_0 is applied in the $+x$ direction, giving the gyro-magnetic anisotropy to YIG material, with the permeability tensor taking the form

$$\overleftrightarrow{\mu}_m = \begin{pmatrix} 1 & 0 & 0 \\ 0 & \mu_1 & \mathrm{i}\mu_2 \\ 0 & -\mathrm{i}\mu_2 & \mu_1 \end{pmatrix}, \tag{1}$$

with

$$\mu_1 = 1 + \frac{\omega_m(\omega_0 - \mathrm{i}\nu\omega)}{(\omega_0 - \mathrm{i}\nu\omega)^2 - \omega^2}, \tag{2}$$

$$\mu_2 = \frac{\omega_m\omega}{(\omega_0 - \mathrm{i}\nu\omega)^2 - \omega^2}, \tag{3}$$

where ω is the angular frequency, $\omega_0 = 2\pi\gamma H_0$ (where γ is the gyro-magnetic ratio) is the procession angular frequency, ω_m is the characteristic circular frequency, and $\nu = \gamma\Delta H/(2\omega)$ is the damping coefficient (where ΔH is

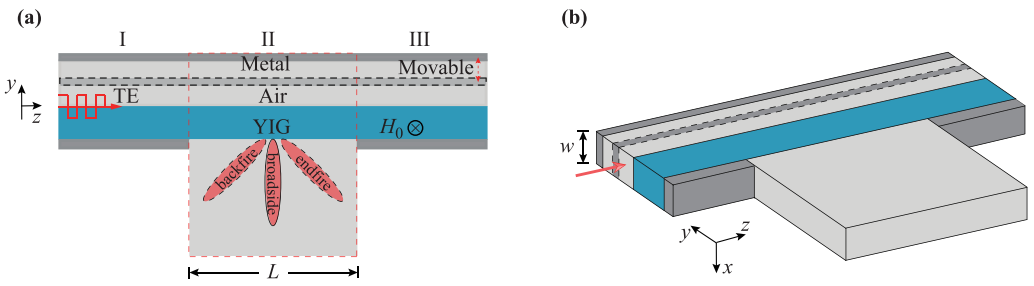


Fig. 1 Schematics of the mechanically scanned Leaky-wave antenna for **(a)** 2D structure, **(b)** 3D structure, where the beam scanning angle is controllable from backfire, broadside to endfire by moving the metal slab. The red dashed frame in (a) is the leaky system composed of a metal-air-YIG-metal-air waveguide.

the resonance linewidth). For system II in Fig. 1(a), the nonzero component of the electric field (E_x) can be written as

$$E_x(z,y) = [A_1 \exp(-\alpha_a y) + A_2 \exp(\alpha_a y)] \exp[\mathrm{i}(\beta z - \omega t)] \tag{4}$$

in the upper air layer for $0 < y \le d_a$, and

$$E_x(z,y) = [B_1 \exp(\alpha_y y) + B_2 \exp(-\alpha_y y)] \exp[\mathrm{i}(\beta z - \omega t)] \tag{5}$$

in the YIG layer for $-d_y < y \le 0$, and

$$E_x(z,y) = C \exp(\alpha_a y) \exp[\mathrm{i}(\beta z - \omega t)] \tag{6}$$

in the lower air layer for $y \le -d_y$, where β is the propagation constant, $\alpha_a = \sqrt{\beta^2 - \varepsilon_a \beta_0^2}$ with $\beta_0 = \omega/c$ (where c is the light speed in vacuum), and $\alpha_y = \sqrt{\beta^2 - \varepsilon_y \mu_v \beta_0^2}$ with $\mu_v = \mu_1 - \mu_2^2/\mu_1$ being the Voigt permeability. Based on boundary conditions at metal-air and air-YIG interfaces, the dispersion relations can be obtained as

$$\left(\alpha_y^2 - \beta^2 \frac{\mu_2^2}{\mu_1^2} - \beta \frac{\mu_2}{\mu_1} \alpha_a \mu_v\right) \tanh(\alpha_a d_a) \tanh(\alpha_y d_y) + \left(\alpha_a \mu_v + \beta \frac{\mu_2}{\mu_1}\right) \tanh(\alpha_y d_y) + \alpha_a \alpha_y \mu_v \tanh(\alpha_a d_a) + \alpha_a \alpha_y \mu_v = 0 \tag{7}$$

for guiding modes with $\beta > |\beta_0|$. It becomes

$$\left(\mathrm{i}\alpha_y^2 - \mathrm{i}\beta^2 \frac{\mu_2^2}{\mu_1^2} - \beta \frac{\mu_2}{\mu_1} p \mu_v\right) \tan(p d_a) \tanh(\alpha_y d_y) + \left(p\mu_v + \mathrm{i}\beta \frac{\mu_2}{\mu_1}\right) \tanh(\alpha_y d_y) + p\alpha_y \mu_v \tan(p d_a) + p\alpha_y \mu_v = 0 \tag{8}$$

for regular modes with $\beta < |\beta_0|$, where $p = \sqrt{\beta_0^2 - \beta^2}$. The regular mode is guided by the mechanism of total reflections at the metal surface and YIG-air interface [30]. Due to the high permittivity of the YIG material, the guiding mode which is surface mode will propagate along the dielectric interface, while the regular mode will be leaked out via the YIG layer when it is thin enough; the latter is called leaky modes which is of interest in this paper. The dispersion curves for guiding modes and leaky modes are displayed in Fig. 2(a) when $H_0 = 1784$ G and $\Delta H = 0$. The air layer and YIG layer are, respectively, set as $d_a = 3$ mm, $d_y = 1.8$ mm.

Figure 2(a) shows the dispersion curves for leaky mode (solid line) and guiding mode (dotted lines). The leaky mode exhibits a positive group velocity ($\mathrm{d}\omega/\mathrm{d}\beta$) within the light cone (dashed lines), and its dispersion band links with the guiding mode bands at points of $\omega = c|\beta|$. At $f = 7.74$ GHz, β becomes zero and the leaky mode is characterized by an infinite phase velocity (ω/β). Notably, since there is a linear term with respect to β in Eq. (7), the leaky mode is nonreciprocal as shown in Fig. 2(a). Assuming that the waveguide width is far less than the vacuum wavelength, the propagating modes associated with the dispersion relation in such a 2D system should have almost the same properties as that in an equivalent 3D system [29, 31]. To verify this, we numerically solved the modes for the 3D system with width of 3 mm, i.e., $0.05\lambda_m$, using the finite element method (FEM), see open circles in Fig. 2(b), which agrees well with that for 2D system. Besides frequency, β is sensitive to the external bias H_0 as well. Figure 2(c) shows the dependence of H_0 on β for leaky mode at a fixed frequency $f = 7.58$ GHz. The relation curve for bias also passes through $\beta = 0$ at $H_0 = 1750$ G and connects to light lines. To identify guiding mode and evanescent mode, the material loss is set at zero in calculating dispersion, while it will be taken into consideration later when we conduct wave transmission.

3 Fixed-bias frequency and fixed-frequency bias beam scanning LWAs

Because the dispersion curve for leaky mode in Figs. 2(b) and (c) possesses monotonous group velocity and passes through $\beta = 0$, our system can support both left-handed (anti-parallel phase and group velocity) and right-handed (parallel phase and group velocity) transmission [28]. This indicates that the proposed LWA possesses backfire-to-endfire scanning, where the main beam scanning angle follows the well-known law

$$\theta_{\mathrm{peak}}(\omega, H_0) = \arcsin(\beta(\omega, H_0)/k_0). \tag{9}$$

From Eq. (9), it is clearly that we can manipulate the beam scanning angle by engineering the frequency ω as well as bias H_0, which are so-called fixed-bias frequency sweep and fixed-frequency bias sweep. For example, when $-\beta_0 \le \beta < 0$, the backward beam scanning can be achieved as $-90^\circ \le \theta_{\mathrm{peak}} < 0$ by changing ω or H_0; when $0 < \beta \le \beta_0$, the forward beam scanning is obtained as $0 < \theta_{\mathrm{peak}} \le 90^\circ$; remarkably when $\beta = 0$, a broadside radiation could be achieved, i.e., $\theta_{\mathrm{peak}} = 0^\circ$. To clarify the backfire-to-endfire scanning feature, we conduct the simulations with various frequencies at fixed-bias and various biases at fixed-frequency by using COMSOL Multiphysics. The parameters are set as: $d_a = 3$ mm, $d_y = 1.8$ mm and $\Delta H = 10$ Oe, $L = 500$ mm. Figures 3(a) and (b) illustrate the evolution of far-field radiation patterns versus frequency at $H_0 = 1784$ G and versus bias at $f = 7.58$ GHz, respectively. It is shown that the beam scanning angle θ can be controlled from backward, broadside, to

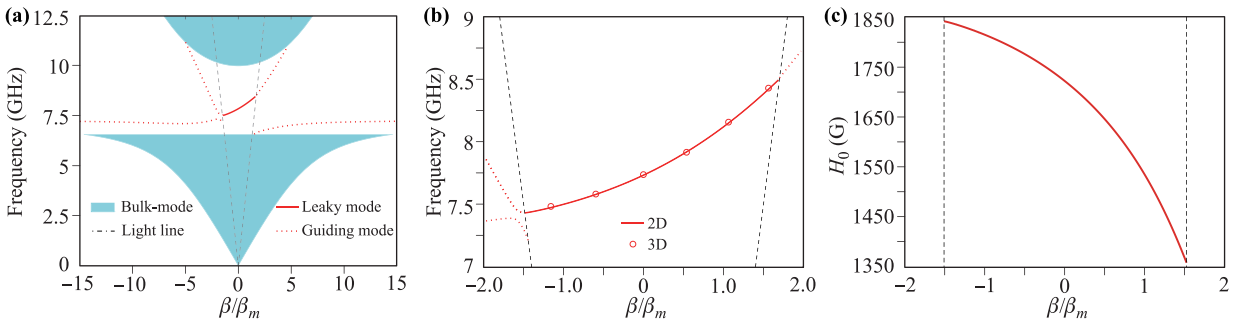


Fig. 2 **(a)** Dispersion relations for leaky mode (solid line) and guiding mode (dotted line). Dashed lines represent the light lines, and the two shaded areas are the zones of bulk modes in the YIG material. **(b)** Magnified view of the leaky mode for 2D (solid lines) and 3D (open circles) structures. **(c)** The dependence of bias on propagation constant for leaky mode. The parameters are $d_a = 3$ mm, $d_y = 1.8$ mm and $H_0 = 1784$ G, $\Delta H = 0$ Oe.

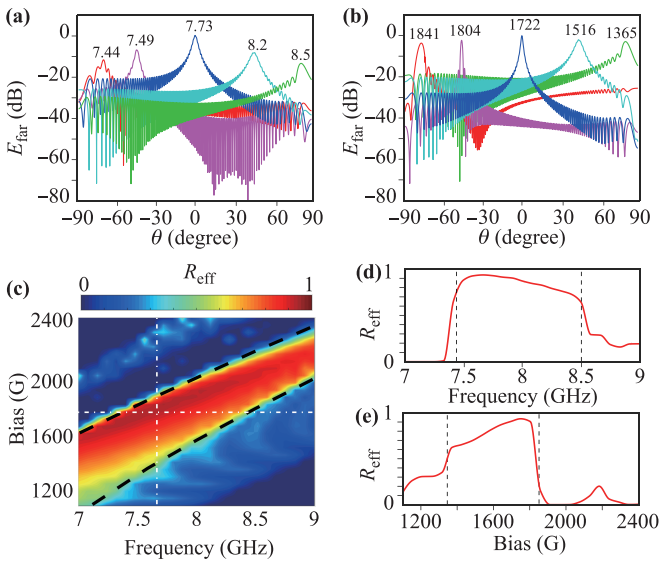


Fig. 3 **(a)** Normalized far-field radiation patterns with continuous frequency scanning at $H_0 = 1784$ G. Numbers inside are the value of frequency (in GHz). **(b)** Normalized far-field radiation patterns with continuous bias scanning at $f = 7.58$ GHz. Numbers inside are the value of bias (in G). **(c)** Leakage radiation efficiency R_{eff} changes with f from 7 GHz to 9 GHz and H_0 from 1100 G to 2400 G. The dashed lines are the contour lines for leaky mode. **(d)** R_{eff} changes with f for a fix $H_0 = 1784$ G, corresponding to the horizontal line in (c). **(e)** R_{eff} changes with H_0 for a fix $f = 7.58$ GHz, corresponding to vertical line in (c). The other parameters are: $d_a = 3$ mm, $d_y = 1.8$ mm and $\Delta H = 10$ Oe, $L = 500$ mm.

forward direction by changing frequency as well as bias. Moreover, We sweep f from 7 GHz to 9 GHz and sweep H_0 from 1100 G to 2400 G to find the corresponding leakage radiation efficiency R_{eff}, see Fig. 3(c), where dashed lines represent the contour line for leaky mode. The efficiency profile indicates that R_{eff} is much higher within leaky mode regime and the maximum efficiency is 94%. The sporadic bright block at the upper left corner refers to the high-order bulk-mode within light lines, while bright slice at the lower right corner suggests the scattered energy arising from the coupling between guiding-part and leak-part. Figure 3(d) shows that, for a fix $H_0 = 1784$ G (see the horizontal line in Fig. 3(c)), the highest value of R_{eff} at $f = 7.74$ GHz, which is consistent with the result in Fig. 2(a). Figure 3(e) shows that, for a fix $f = 7.58$ GHz [see the vertical line in Fig. 3(c)], the highest value of R_{eff} is at $H_0 = 1750$ G.

4 Mechanically scanned LWAs at a fixed frequency and fixed bias

For the present MAYA system, the dispersion curves should not be only sensitive to the bias H_0, but also closely depends on the thickness of air layer d_a. Figure 4(a) shows the dispersion relations for leaky mode at various d_a. It is seen that the dispersion curves shift down when increasing d_a. Here we choose a fixed bias of $H_0 = 1784$ G, fixed frequency of $f = 7.58$ GHz as an example, see the horizontal dot-dashed line in Fig. 4(a). Figure 4(b) indicates the dependence of air thickness on propagation constant. When changing the air thickness from 2.55 mm to 9 mm, β can be controlled from $-\beta_0$ to β_0. The dispersion curves can be tuned by air thickness, giving us an opportunity to manipulate the beam scanning angle by engineering the air thickness. To clarify the mechanically controlled feature, we construct LWAs with different d_a when $H_0 = 1784$ G, $f = 7.58$ GHz. The other parameters are: $\Delta H = 10$ oe, $d_y = 1.8$ mm, and $L = 500$ mm. Figure 4(b) shows the evolution of far-field radiation patterns E_{far} versus air thickness.

Like fixed-bias frequency and fixed-frequency bias sweep in our LWA, the proposed mechanically controlled LWAs also can achieve continuous beam scanning, which is from backward, broadside, to forward direction. In addition, the dispersion curve for leaky mode can also be tuned by changing the YIG thickness d_y. However, when d_y is bigger than a certain value, the dispersion curve almost keeps the same, leading to a small scanning range.

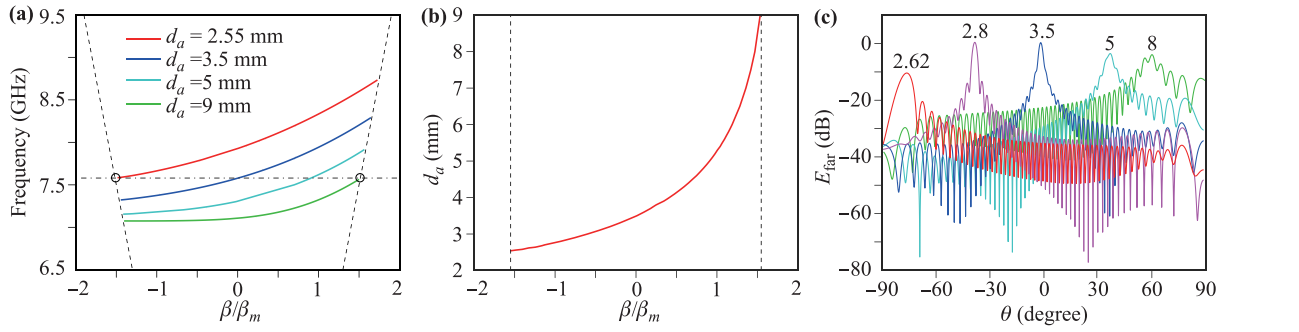


Fig. 4 **(a)** Dispersion relations of leaky mode for various air thickness. The horizontal dot-dashed line shows the fixed frequency of $f = 7.58$ GHz. **(b)** The dependence of air thickness on propagation constant. **(c)** Normalized far-field radiation patterns with continuous air thickness scanning. Numbers inside are the value of thickness (in mm). The bias is fixed at 1784 G.

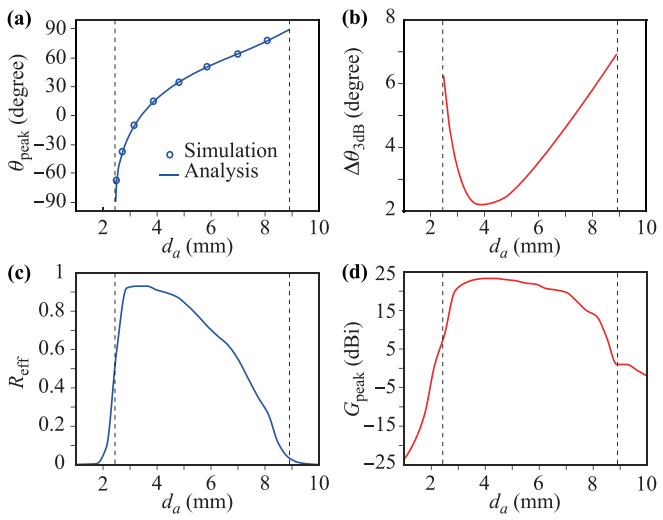


Fig. 5 **(a)** The simulated (circles) and analytic (solid line) results of θ_{peak}, **(b)** $\Delta\theta_{3\text{dB}}$, **(c)** R_{eff}, and **(d)** G_{peak} vs. d_a.

Figure 5(a) illustrates the peak of simulated beam scanning angle θ_{peak}, see open circles, and analytic θ_{peak}, see solid line, as a function of d_a, showing a good agreement with each other. For analytic results, θ_{peak} is found to be $-90°$ when $d_a = 2.5$ mm; θ_{peak} is $90°$ when $d_a = 9$ mm. The scanning range for simulated results reaches as high as 149°, which is smaller than the analytic results. It can be explained by the fact that the mesh restraint of finite element method limits the calculation accuracy. Figure 5(b) shows the 3dB beam width $\Delta\theta_{3\text{dB}}$ versus with d_a, corresponding to the beam width when the maximum value of E_{far} drops a value of 3dB. The average $\Delta\theta_{3\text{dB}}$ is as low as $4.6°$ and the minimum is found to be $2.2°$ when $d_a = 4$ mm. The leakage radiation efficiency versus thickness is given in Fig. 5(c). It can be found that R_{eff} remains extremely higher for leaky mode (see dashed lines), especially when the dispersion curve is far away from light lines and the maximum value of 94% appears at $d_a = 4$ mm. Moreover, we also calculate the peak of antenna gain G_{peak} versus d_a [see Fig. 5(d)], showing G_{peak} reaches 23 dBi at $d_a = 4$ mm. G_{peak} remains 20 dBi from $d_a = 2.8$ mm to $d_a = 7$ mm, and it gradually decreases both in forward and backward directions when changing the air thickness.

To further show the field profile for our uniform LWA, the simulated electric field E_x amplitudes in 2D and 3D systems are presented in Figs. 6(a–f). Figures 6(a–c) illustrate, respectively, E_x amplitudes in 2D system for three typical cases, associating with Figs. 6(d–f) are E_x amplitudes in 3D system. In the simulation, the width of the 3D system in the x direction is 3 mm, and the loss $\Delta H = 10$ Oe is taken into account. The other parameters are: $d_y = 1.8$ mm, $f = 7.58$ GHz and $H_0 = 1784$ G. It is

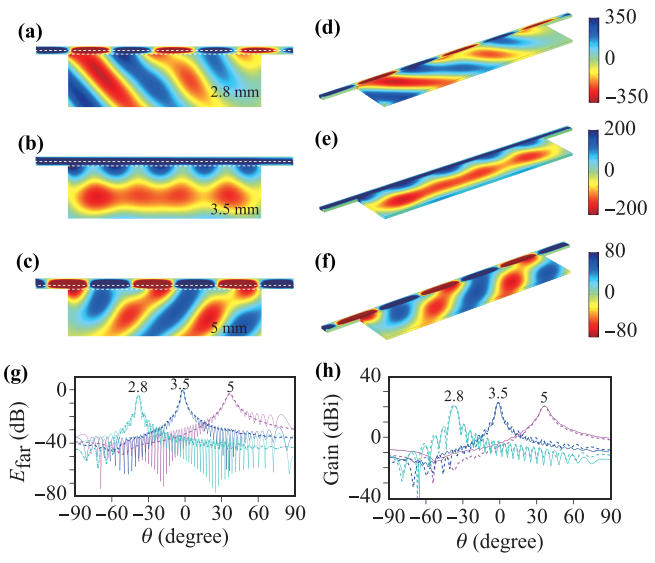


Fig. 6 Simulated electric field E_x amplitudes in 2D system for **(a)** $d_1 = 2.8$ mm, **(b)** $d_1 = 3.5$ mm, and **(c)** $d_1 = 5$ mm. **(d–f)** E_x amplitude in 3D system corresponding to (a–c), respectively. **(g)** Normalized far-field radiation patterns and **(h)** gain with three typical air thickness. Solid lines and dashed lines in Figs. 6(g) and (h) represent the patterns in 2D system and 3D system, respectively. The other parameters are $d_2 = 1.8$ mm, $H_0 = 1784$ G and $\Delta H = 10$ Oe.

seen that the electromagnetic energy in the two systems is leaked out through the YIG layer and exhibits forward radiation for $d_a = 2.8$ mm, broadside radiation for $d_a = 3.5$ mm, and backward radiation for $d_a = 5$ mm, which are well consistent with the results stated in Fig. 4(b). The normalized far-field radiation patterns and antenna gains for 3D system in the yz plane are shown in Figs. 6(g) and (h), see dashed lines. For comparison, the corresponding results for 2D system are plotted as solid lines. As expected, the far-field radiation patterns and antenna gains for the 2D and 3D systems agree well, showing the same directionality and field intensity.

5 Conclusion

In summary, we have proposed a uniform backfire-to-endfire leaky-wave antenna constructed by novel metal-air-YIG-air waveguide under bias magnetic field. The structure supports leaky modes guided by the total internal reflections at the metal surface and YIG-air interface. We systemically analyze the dispersion relation, showing that the propagation constant can be manipulated by changing frequency as well as bias. The fixed-bias frequency and fixed-frequency bias scanned LWAs exhibit continuous beam scanning from backward, broadside to forward. More importantly, we for the first time propose a backfire-to-endfire beam scanning LWA enabled mechanically controlling, where the dispersion relation is controllable by air thickness. By manipulating the air thickness, the beam scanning range reaches as high as 149° with low average 3dB beam of 4.6°, and the radiation efficiency is up to 94% with the maximum gain of 23 dBi. Because of the uniform and multilayered structure, mechanically controlled LWA is super easy to be fabricated, where the air thickness can be tuned by move the upper metal slab straightforwardly. Being provided with multiple controlled (specially mechanically) scanning manners, the present LWA has an active potential to be an ideal alternative to various application including modern communication and radar system.

Acknowledgements This work was supported by the National Natural Science Foundation of China (NSFC) (Grant No. 61372005), the National Natural Science Foundation of China (NSFC) under the key project (Grant No. 41331070), the Natural Science Foundation of Ningbo (No. 2019A610081), and Zhejiang Provincial Natural Science Foundation of China (No. LY20F050006).

References

1. W. W. Hansen, U.S. Patent 2 402 622 (1940)
2. D. Comite, S. K. Podilchak, P. Baccarelli, P. Burghignoli, A. Galli, A. P. Freundorfer, and Y. M. M. Antar, Analysis and design of a compact leaky-wave antenna for wide-band broadside radiation, *Sci. Rep.* 8(1), 17741 (2018)
3. J. L. Gomez-Tornero, Analysis and design of conformal tapered leaky-wave antennas, *IEEE Antennas Wirel. Propag. Lett.* 10, 1068 (2011)
4. L. Wang, J. L. Gomez-Tornero, E. Rajo-Iglesias, and O. Quevedo-Teruel, Low-dispersive leaky-wave antenna integrated in Groove gap waveguide technology, *IEEE Trans. Antenn. Propag.* 66(11), 99 (2018)
5. J. Xu, W. Hong, H. Tang, Z. Kuai, and K. Wu, Half-mode substrate integrated waveguide (HMSIW) leaky-wave antenna for millimeter-wave applications, *IEEE Antennas Wirel. Propag. Lett.* 7, 85 (2008)
6. D. R. Jackson, C. Caloz, and T. Itoh, Leaky-wave antennas, *IEEE Proc.* 100(7), 2194 (2012)
7. Q. Song, S. Campione, O. Boyraz, and F. Capolino, Silicon-based optical leaky wave antenna with narrow beam radiation, *Opt. Express* 19(9), 8735 (2011)
8. J. L. Gomez-Tornero, D. Blanco, E. Rajo-Iglesias, and N. Llombart, Holographic surface leaky-wave lenses with circularly-polarized focused near-fields (I): Concept, design and analysis theory, *IEEE Trans. Antenn. Propag.* 61(7), 3475 (2013)
9. A. Lai, C. Caloz and T. Itoh, Composite right/left-handed transmission line metamaterials, *IEEE Microw. Mag.* 5(3), 34 (2004)
10. J. Y. Yin, J. Ren, Q. Zhang, H. C. Zhang, Y. Q. Liu, Y. B. Li, X. Wan, and T. Jun Cui, Frequency-controlled broad-angle beam scanning of patch array fed by Spoof surface plasmon polaritons, *IEEE Trans. Antenn. Propag.* 64(12), 5181 (2016)
11. L. Liu, C. Caloz, and T. Itoh, Dominant mode leaky-wave antenna with backfire-to-endfire scanning capability, *Electron. Lett.* 38(23), 1414 (2002)
12. L. Goldstone and A. Oliner, Leaky-wave antennas (I): Rectangular waveguides, *IEEE Trans. Antenn. Propag.* 7(4), 307 (2003)
13. W. Hong, T. L. Chen, C. Y. Chang, J. W. Sheen, and Y. D. Lin, Broadband tapered microstrip leaky-wave antenna, *IEEE Trans. Antenn. Propag.* 51(8), 1922 (2003)
14. M. Wang, H. F. Ma, H. C. Zhang, W. X. Tang, X. R. Zhang, and T. J. Cui, Frequency-fixed beam-scanning leaky-wave antenna using electronically controllable corrugated microstrip line, *IEEE Trans. Antenn. Propag.* 66(9), 4449 (2018)
15. M. Wang, H. F. Ma, W. X. Tang, H. C. Zhang, W. X. Jiang, and T. J. Cui, A dual-band electronic-scanning leaky-wave antenna based on a corrugated microstrip line, *IEEE Trans. Antenn. Propag.* 67(5), 3433 (2019)
16. D. K. Karmokar, K. P. Esselle, and S. G. Hay, Fixed-frequency bBeam steering of microstrip leaky-wave Antennas using binary switches, *IEEE Trans. Antenn. Propag.* 64(6), 2146 (2016)
17. R. Guzman-Quiros, J. L. Gomez-Tornero, A. R. Weily, and Y. J. Guo, Electronically steerable 1-D Fabry–Perot leaky-wave antenna employing a tunable high impedance surface, *IEEE Trans. Antenn. Propag.* 60(11), 5046 (2012)

18. B. Lax and K. J. Button, Microwave Ferrites and Ferrimagnetics, New York, 1962
19. A. Hartstein, E. Burstein, A. A. Maradudin, R. Brewer, and R. F. Wallis, Surface polaritons on semi-infinite gyromagnetic media, *J. Phys. C* 6(7), 1266 (1973)
20. T. Kodera and C. Caloz, Integrated leaky-wave antenna–duplexer/diplexer using CRLH uniform ferrite-loaded open waveguide, *IEEE Trans. Antenn. Propag.* 58(8), 2508 (2010)
21. T. Ueda and M. Tsutsumi, Left-handed transmission characteristics of rectangular waveguides periodically loaded with ferrite, *IEEE Trans. Magn.* 41(10), 3532 (2005)
22. T. Ueda and M. Tsutsumi, Nonreciprocal left-handed transmission characteristics of microstriplines on ferrite substrate, *IET Microw. Antennas Propag.* 1(2), 349 (2007)
23. Z. Y. Li, Nanophotonics in China: Overviews and highlights, *Front. Phys.* 7(6), 601 (2012)
24. R. Wang, X. G. Ren, Z. Yan, L. J. Jiang, W. E. I. Sha, and G. C. Shan, Graphene based functional devices: A short review, *Front. Phys.* 14(1), 13603 (2019)
25. A. B. Khanikaev and G. Shvets, Two-dimensional topological photonics, *Nat. Photonics* 11(12), 763 (2017)
26. S. C. Zhang, Z. Fang, and Q. K. Xue, Advances in topological materials, *Front. Phys.* 7(2), 147 (2012)
27. T. Ozawa, H. M. Price, A. Amo, N. Goldman, M. Hafezi, L. Lu, M. C. Rechtsman, D. Schuster, J. Simon, O. Zilberberg, and I. Carusotto, Topological photonics, *Rev. Mod. Phys.* 91(1), 015006 (2019)
28. T. Kodera and C. Caloz, Uniform ferrite-loaded open waveguide structure with CRLH response and its application to a novel backfire-to-endfire leaky-wave antenna, *IEEE Trans. Microw. Theory Tech.* 57(4), 784 (2009)
29. Q. Shen, L. F. Shen, W. D. Min, C. Wu, X. H. Deng, and S. S. Xiao, Trapping a magnetic rainbow by using a one-way magnetostatic-like mode, *Opt. Mater. Express* 9(11), 4399 (2019)
30. X. Deng, L. Hong, X. Zheng, and L. Shen, One-way regular electromagnetic mode immune to backscattering, *Appl. Opt.* 54(14), 4608 (2015)
31. Q. Shen, L. J. Hong, X. H. Deng, and L. F. Shen, Completely stopping microwaves with extremely enhanced magnetic fields, *Sci. Rep.* 8(1), 15811 (2018)